

# Towards Co-operative Beaming Displays: Dual Steering Projectors for Extended Projection Volume and Head Orientation Range

Hiroto Aoki , Takumi Tochimoto , Yuichi Hiroi , and Yuta Itoh 

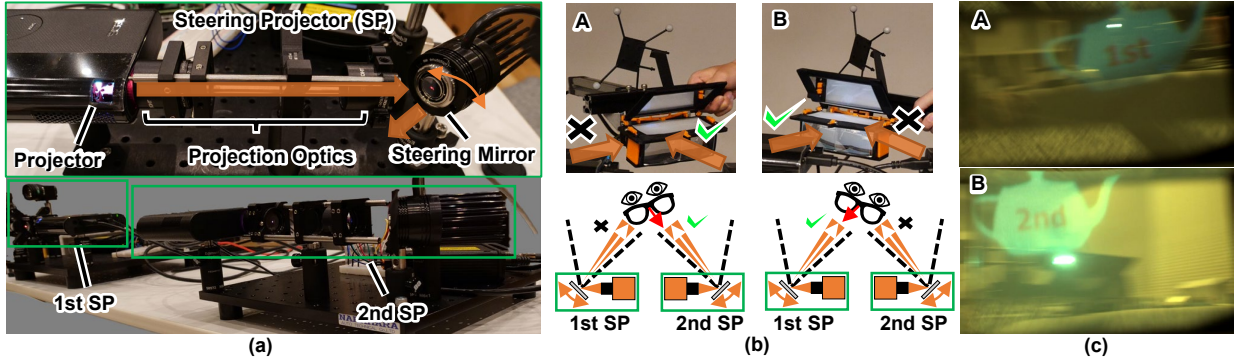


Fig. 1: Overview of our dual-beaming display system where dual steering projectors dynamically cooperate in an outside-in tracking environment. (a) The front view of our steering projectors in the scene. We placed two steering projectors to present images from a distance. (b top) An view of the posture of the passive headset taken from an external viewpoint. (b bottom) a schematic of the relative posture of the passive headset and steering projectors. (c) Images captured from the user-perspective camera placed behind the headset. With one steering projector, the head orientation and the scene volume that the headset can receive images from the string projectors are limited. Our dual steering projectors working collaboratively address these constraints.

**Abstract**—Existing near-eye displays (NEDs) have trade-offs related to size, weight, computational resources, battery life, and body temperature. A recent paradigm, beaming display, addresses these trade-offs by separating the NED into a steering projector (SP) for image presentation and a passive headset worn by the user. However, the beaming display has issues with the projection area of a single SP and has severe limitations on the head orientation and pose that the user can move. In this study, we distribute dual steering projectors in the scene to extend the head orientation and pose of the beaming display by coordinating the dual projections on a passive headset. For cooperative control of each SP, we define a geometric model of the SPs and propose a calibration and projection control method designed for multiple projectors. We present implementations of the system along with evaluations showing that the precision and delay are  $1.8 \sim 5.7$  mm and 14.46 ms, respectively, at a distance of about 1 m from the SPs. From this result, our prototype with multiple SPs can project images in the projection area ( $20 \text{ mm} \times 30 \text{ mm}$ ) of the passive headset while extending the projectable head orientation. Furthermore, as applications of cooperative control by multiple SPs, we show the possibility of multiple users, improving dynamic range and binocular presentation.

**Index Terms**—Near-eye display, Augmented reality, Projectors

## 1 INTRODUCTION

Near-eye displays (NEDs) are the primary device for augmented reality (AR) [10]. Their popularity has increased since the launch of commercial products like Microsoft HoloLens and Magic Leap. Nevertheless, their trade-offs concerning size, weight, computational resources, battery life, body temperature etc., prevent the community from realizing the ultimate NEDs practical for daily use.

Itoh et al. introduced a new NED paradigm called the Beaming Display, which attempts to address the above critical design trade-offs [7]. This paradigm divides the NED into two components: a remote steering projector that projects virtual images from a distance, and a passive

headset worn by the user. The steering projector includes a projector, a steering mirror, and a tracking camera that estimates the position and pose of the passive headset. In contrast to conventional NEDs, computational resources and batteries are mounted on the steering projector installed in the environment, rather than on the passive headset. As a result, the passive headset can be smaller and lighter, without restrictions on battery capacity or computational resources [1]. Moreover, this configuration eliminates thermal issues near the user's skin. These benefits potentially enable prolonged usage of AR applications.

The initial prototype of the beaming display has validated the feasibility of the concept by achieving a resolution comparable to consumer VR headsets. However, their prototype with a coaxial tracking camera on the steering projector and an AR marker on the headset limit the tracking speed and the projection volume, which delineates the space where the user can receive images and restricts head orientation to a single direction. To be specific, their projection volume was confined to a cone range of  $30 \times 30$  degrees from the steering projector, with a maximum projection distance of 2 meters. Furthermore, the restriction on head orientation allowed only a 20-degree rotation from the user's gaze towards the steering projector.

The head orientation and projection volume can be expanded by coordinating multiple steering projectors to project onto the passive headset. Fortunately, increasing the number of steering projectors

• Hiroto Aoki is with The University of Tokyo. E-mail: [aoki-hiroto633@g.ecc.u-tokyo.ac.jp](mailto:aoki-hiroto633@g.ecc.u-tokyo.ac.jp).  
 • Takumi Tochimoto is with Tokyo Institute of Technology. E-mail: [takumi.tochimoto@arc.titech.ac.jp](mailto:takumi.tochimoto@arc.titech.ac.jp).  
 • Yuichi Hiroi is with Cluster Metaverse Lab. E-mail: [y.hiroi@cluster.mu](mailto:y.hiroi@cluster.mu).  
 • Yuta Itoh is with The University of Tokyo. E-mail: [yuta.itoh@iii.u-tokyo.ac.jp](mailto:yuta.itoh@iii.u-tokyo.ac.jp).

This work has been submitted to the IEEE for possible publication. Copyright may be transferred without notice, after which this version may no longer be accessible.

will not affect the size or weight of the passive headset, although it will increase the resources on the environmental side. However, in practice, realizing such a system is difficult due to various calibration requirements. This work thus addresses the current limitation of the beaming display by constructing it with two steering projectors with dual axis mirrors and an outside-in tracking environment.

To control multiple steering projectors cooperatively, we propose a method to model and calibrate the projectors and steering mirrors that compose the steering projector in three-dimensional geometry. As described in Sec. 2.1, previous studies have calibrated based on models that do not consider the steering mirror and are unsuitable for the cooperative control of multiple units. Although this study constructs a system with two steering projectors, the optical design of the proposed system, the newly formulated geometric calibration methods for various coordinate systems, and the implementation of the control system can be naturally applied to systems with more than two steering projectors, thus ensuring scalability.

The main contributions of this study are:

- Modeling/evaluating spatial calibration and projection control for multi-beaming display with outside-in tracking.
- Validating the extension of the head orientation and the working volume of the headset by the dual steering projectors.
- Demonstrating potential applications of the system beyond extending the head orientation and the working volume.
- Providing insights and discussion towards practical systems.

## 2 RELATED WORK

Our work is closely related to dynamic projections in spatial AR or projection mapping. This section thus focuses on reviewing projection research and omitting works on NED optics. Readers interested in NED optics are referred to the review papers [10, 11].

Projection mapping is a type of AR that projects virtual images onto the surface of a real object. When the projected object moves, it is called dynamic projection mapping (DPM). Beaming display is conceptually similar to DPM, as it projects virtual images from a projector onto a moving passive headset. However, there are essential differences, including the small size of the projection screen (e.g.,  $20 \times 30$  mm in the current prototype), the fact that the projection screen is part of the passive headset worn by the user, and the ability to provide a large field of view without requiring a large space.

Despite these differences, the DPM configuration and algorithms can be adapted to the beaming display. The following sections describe previous studies that extend the projection area of the DPM and compare them with the proposed system.

### 2.1 Dynamic projection with steering devices

In computer vision, a pan-tilt-zoom (PTZ) camera is a popular steering mechanism [30]. For high-speed optical steering including our use case, however, applying the PTZ camera model is deemed unsuitable owing to misalignment between mechanical and optical centers [23]. Unlike PTZ cameras, a mirror device, such as a galvanometer or steering mirror, can dynamically control the optical axis of a camera or projector in high-speed.

The saccade mirror is an optical axis control system that uses a mirror device and pupil shift lens. Thanks to its light weight, unlike mechanical steering systems [34], the saccade mirrors can achieve high-speed optical steering such as active vision [23]. A pupil shift lens transfers the camera's optical center between the mirror surfaces of the galvanometer mirror, allowing for the high-speed control of the optical axis [16]. This enables the capture of fast-moving objects at an appropriate angle of view without blur.

Several studies have used high-speed active vision with saccade mirrors to project images onto fast-moving objects [16, 17, 24, 28]. In these studies, a high-speed camera and a projector are coaxially positioned, and galvanometer mirrors control their optical axes to project onto a dynamic object with almost no time lag. In addition, by controlling the optical axis of the projector with a mirror device, the amount of

light and resolution for the projection area is improved [21]. Expanding the projection area using a mirror device is compatible with a beaming display, which projects to a small screen. The existing prototype also uses a steering mirror to control the optical axis [7]. However, one issue is that the screen must be oriented toward the steering mirror to project appropriately.

### 2.2 Dynamic projection with multiple projectors

Several prior studies have used multiple projectors to project images onto moving objects [22, 26]. Multiple projectors allow for expansion of the mapping area, removal of shadows, and expansion of the dynamic range of luminance [26]. In beaming displays, multiple projectors can be distributed across a space to increase the angle of rotation of the screen so that the screen can receive virtual images. However, to ensure sufficient light intensity and resolution of the image projected on the beaming display's small passive screen, the projectors' angle of view must be small. Therefore, to cover all of the user's projection volume simply by increasing the number of projectors, it is necessary to have many with a narrow angle of view.

### 2.3 DPM system calibration technique

DPM systems need to identify static/dynamic coordinates to project light onto desired locations. This calibration is often specific to each configuration and the procedure may require dedicated procedures.

As in Sec. 2.1, existing mirror device DPM [16, 17, 24, 28] and beaming display [7] employ coaxial procam systems [35], in which the projector and tracking camera are placed on different sides of a half-mirror. The coaxial procam system facilitates alignment with the projection target because the correspondence between each pixel of the projector and camera is constant. However, these studies use projection control by obtaining 2D offsets from the tracking camera frame and do not estimate the relative 6 degrees-of-freedom (6DoF) pose between the projector, mirror device, and projection target. To coordinate multiple projectors in our setup, we need this 6DoF pose. Thus, we use an external non-coaxial tracking camera to calibrate the steering projectors in 3D geometry.

There is a DPM with 3D calibration of the mirror device. Mikawa et al. proposed an aerial image presentation system that uses a galvanometer mirror to scan a laser beam to the user's pupil to realize an aerial display for distant users [15]. Their work uses a non-coaxial camera to track the user's pupil, and they calibrated the entire system in three dimensions so that the laser can be aimed at it. However, the prototype in this study is limited to presenting images at only one point. To apply it to image presentation in a beaming display, scanning the laser at high speed or using a projector as the image presentation device is necessary. Therefore, we developed a calibration procedure by projecting images on the screen by calibrating the projector and steering mirror in 3D geometry.

## 3 PROJECTION CONTROL OF STEERING PROJECTORS

This section describes the steering projector used in the proposed system. First, the geometric model of the steering projector is described in Sec. 3.2. Then, the overall calibration procedure is described in Sec. 3.3. Finally, the projection control of the steering projector is described in Sec. 3.4.

Our geometric model and calibration of the steering projector are adapted from a steering camera system [27]. They modeled and calibrated a system consisting of a camera and a galvanometer mirror to apply a high-speed optical axis control system to 3D measurement. However, two differences compared to their method exist. First, our system is a projector, not a camera, and we use outside-in tracking for projection targets. Second, we use a 2-axes gimbal steering mirror instead of a galvanometer mirror. Since the mechanism to control the angle of the mirror is different, the calculation to determine the normal vector of the mirror surface is different. Also, unlike the galvanometer mirror, the steering mirror has one mirror, so the coordinate system of the projector reflected in the mirror is inverted between the right-hand and left-hand systems.

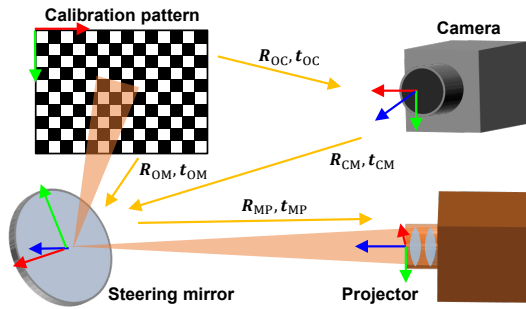


Fig. 2: Geometric model of the system consisting of a projector with relay optics, a two-axes steering mirror, a calibration camera, and a calibration pattern.

Note that the common PTZ camera model is inappropriate in our use case because steering projectors have three distinct centers: mechanical, mirror surface, and relay optics center, which do not generally coincide unlike in the PTZ model.

### 3.1 Notations

Throughout the rest of this paper, coordinate systems are treated as right-handed. Bold lower/upper-case letters denote vectors/matrices such as  $X, x$ . Homogeneous coordinate of  $x$  is denoted as  $\tilde{x}$ . Lowercase letters denote scalars. Uppercase letters denote a coordinate system such as  $A$ . Given a coordinate system  $A$ , a 3D point in  $A$  is denoted by vectors with the coordinate symbol as the lower index:  $x_A$ . Given systems  $A$  and  $B$ , the relative transformation from  $[A$  to  $B]$  is represented by  $[R_{AB}, t_{AB}]$ , where  $R_{AB}$  and  $t_{AB}$  denote rotation and translation respectively. The transformation of a 3D point  $x_A$  in  $A$  to  $x_B$  in  $B$  can be written as  $x_B = R_{AB}x_A + t_{AB}$ . When coordinates in  $A$  are distinguished by the variable  $i$ , they are denoted as  $x_{A\{i\}}$ .

### 3.2 Geometric model of steering projector

In this section, we first describe a model in which a single mirror reflects the projector geometry. Next, we describe a model that considers that the steering mirror angle is updated. Finally, a model that includes a non-coaxial camera is described. Fig. 2 shows the geometric model of the proposed system.

#### 3.2.1 Model consisting of projector and mirror

We consider the projector geometry that maps a 3D point to a point on a 2D image plane. The projector model is treated as a pinhole camera model [5] with the light ray direction reversed. Let  $3 \times 4$  matrix  $P_{OP}$  be the projection matrix from the calibration pattern coordinate system  $O$  to the image plane to the projector coordinate system  $P$ . Also, let  $\tilde{x}_O$  be the vector of  $O$  and  $\tilde{x}_P$  be the vector in the image plane of  $P$ . Then, the projective geometry can be expressed with the projection matrix  $P_{OP}$  as:

$$\tilde{x}_P \sim P_{OP}\tilde{x}_O, P_{OP} = K_P[R_{OP}|t_{OP}]. \quad (1)$$

Considering the lens distortion  $D_P(\cdot)$ , and the projector matrix  $K_P$  with the focal length  $f_x, f_y$  and principal point position  $c_x, c_y$ , the projective geometry can be expressed as:

$$\tilde{x}_P \sim K_P D_P([R_{OP}|t_{OP}]\tilde{x}_O), K_P = \begin{bmatrix} f_x & 0 & c_x \\ 0 & f_y & c_y \\ 0 & 0 & 1 \end{bmatrix}. \quad (2)$$

We place one steering mirror in front of the projector, so the reflected projector coordinate system is flipped from the right-hand to the left-hand system. So, the projective geometry is expressed as:

$$\tilde{x}_P \sim K_P D_P([R_{OP}|t_{OP}]\begin{bmatrix} I_z & 0 \\ 0 & 1 \end{bmatrix}\tilde{x}_O), I_z = \begin{bmatrix} 1 & 0 & 0 \\ 0 & 1 & 0 \\ 0 & 0 & -1 \end{bmatrix}. \quad (3)$$

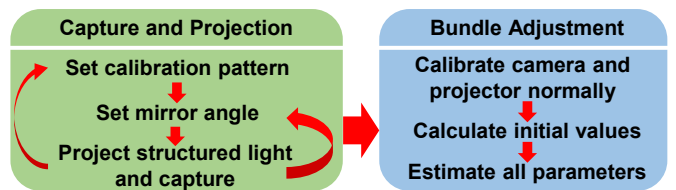


Fig. 3: Overview of the calibration procedure.

#### 3.2.2 Model considering angle update of steering mirror

Let  $l$  be the distance from the origin to the mirror surface and  $n = [a, b, c]^T$  be the unit normal vector of the mirror surface. The mirror transformation matrix can be expressed as:

$$M(n, l) = \begin{bmatrix} M_r(n) & M_t(n, l) \\ 0 & 1 \end{bmatrix} \quad (4)$$

$$M_r(n) = \begin{bmatrix} 1 - 2a^2 & -2ab & -2ac \\ -2ab & 1 - 2b^2 & -2bc \\ -2ac & -2bc & 1 - 2c^2 \end{bmatrix}, M_t(n, l) = \begin{bmatrix} 2la \\ 2lb \\ 2lc \end{bmatrix} \quad (5)$$

where the normal vector is oriented outward from the origin.

Let  $(\alpha, \beta)$  be the specified angle to the mirror. The steering mirror coordinate system  $M$  is as shown in Fig. 2, with the center of rotation of the steering mirror as the origin, the opposite direction of the normal vector at  $(\alpha, \beta) = (0, 0)$  as the  $z$  axis, the rotation axis of the mirror surface are defined as  $x$ -axis and  $y$ -axis. The steering mirror's unit normal vector  $n$  can be expressed as:

$$n = R_y(-\alpha)R_x(\beta)e_{-z} = \begin{bmatrix} \sin \alpha \cos \beta \\ \sin \beta \\ -\cos \alpha \cos \beta \end{bmatrix} \quad (6)$$

where  $e_{-z} = [0, 0, -1]^T$ ,  $R_x(\theta)$  and  $R_y(\theta)$  are rotation matrices that rotate  $\theta$  (rad) around the  $x$ -axes and  $y$ -axes.

Let  $[R_{OM}|t_{OM}]$  be the coordinate transformation from the calibration pattern coordinate system  $O$  to the steering mirror coordinate system  $M$ , and let  $[R_{MP}|t_{MP}]$  be the coordinate transformation from  $M$  to the projector coordinate system  $P$ . The projective geometry can be expressed as:

$$\tilde{x}_P \sim K_P D_P \left( [R_{MP}|t_{MP}]M(n, l) \begin{bmatrix} R_{OM} & t_{OM} \\ 0 & 1 \end{bmatrix} \tilde{x}_O \right) \quad (7)$$

#### 3.2.3 Model including camera

Let  $[R_{OC}|t_{OC}]$  be the transformation from the calibration pattern coordinate system  $O$  to the camera coordinate system  $C$ . Also, let  $[R_{CM}|t_{CM}]$  be the transformation from  $C$  to the steering mirror coordinate system  $M$ . The conversion from  $O$  to  $M$  is equal to conversion from  $O$  to  $M$  via  $C$ . Therefore, the projective geometry of the Eq. (7) can be expressed as:

$$\tilde{x}_P \sim K_P D_P \left( [R_{MP}|t_{MP}]M(n, l) \begin{bmatrix} R_{CM} & t_{CM} \\ 0 & 1 \end{bmatrix} \begin{bmatrix} R_{OC} & t_{OC} \\ 0 & 1 \end{bmatrix} \tilde{x}_O \right) \quad (8)$$

### 3.3 Geometric calibration of steering projectors

The calibration procedure for the parameters defined in Sec. 3.2 is described below. Fig. 3 shows the calibration procedure.

#### 3.3.1 Calibration pattern capture and projection

Fig. 4 shows the capture and projection at calibration. A structured code pattern is projected from the projector onto the calibration pattern and shot from the camera. The projection and capture are repeated while changing the mirror angle  $i$  and the calibration pattern pose  $k$ . This allows us to obtain the coordinates  $\tilde{x}_{C\{jk\}}$  of the camera image plane at each  $k$  corresponding to the coordinates  $\tilde{x}_{O\{jk\}}$  of the calibration pattern in the calibration pattern coordinate system. Also, the coordinates  $\tilde{x}_{P\{ijk\}}$  of the projector image plane at each  $k$  at each  $i, k$  corresponding to  $\tilde{x}_{O\{jk\}}$  can be obtained [19].

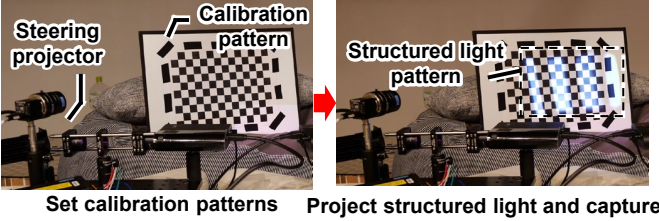


Fig. 4: Capture and projection at calibration.

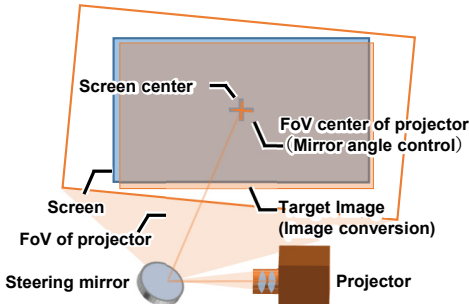


Fig. 5: Steering projector projection control. Aligns the FoV center of the projector with the center of the screen by controlling the angle of the steering mirror. Also, align the corners of the target image with the corners of the screen by image transformation.

### 3.3.2 Normal camera and projector calibration

The camera parameters  $K_C, D_C, R_{OC\{k\}}, t_{OC\{k\}}$  for each  $k$  are obtained by Zhang's method [36]. Also, projector parameters  $K_P, D_P, R_{OP\{ik\}}, t_{OP\{ik\}}$  for each  $i, k$  are obtained by the method of Moreno et al. [19]. When calibrating the projector, the z-coordinate of the coordinate of the calibration point in the calibration pattern coordinate system is set to 0, so there is no need to consider the  $I_z$  in the Eq. (3). This allows us to obtain the calibration parameters similarly to normal projector calibration.

### 3.3.3 Bundle adjustment

Bundle adjustment in this system can be described as the following nonlinear optimization problem.

$$\arg \min_{\xi} \sum_{i,j,k} \left( \frac{d(\tilde{x}_{P\{ijk\}}, \tilde{x}'_{P\{ijk\}})}{N_{i,j,k}} \right)^2, \quad (9)$$

where  $\tilde{x}'_{P\{ijk\}}$  are the calibration point coordinates estimated by Eq. (8),  $\xi$  are the calibration parameters to be estimated,  $d(a, b)$  is the Euclidean distance between vectors  $a, b$ ,  $N_{i,j,k}$  is the number of times the  $j$  point in the pattern pose  $k$  is duplicated at each mirror angle  $i$ . We fix  $K_P, D_P, R_{OP\{ik\}}, t_{OP\{ik\}}$  and solve for  $R_{MP}, t_{MP}, R_{CM}, t_{CM}$  as unknowns. We included Table 1 in Appendix A to summarize the calibration parameters described in this section.

### 3.3.4 Initial value calculation

As explained in the Sec. 3.3.3, the final bundle adjustment solves the nonlinear optimization problem. We employ the Levenberg-Marquardt(LM) method [18]. For the method, we need to estimate the initial values of  $R_{MP}, t_{MP}, R_{CM}$ , and  $t_{CM}$ . The detailed derivation process for each value is described in the supplementary document.

## 3.4 Projection control of steering projectors

This section describes the projection control of the steering projector. Sec. 3.4.1, 3.4.2 describe an algorithm to ensure that a single steering projector properly project the target image to the screen. Sec. 3.4.3 does a method for coordinating multiple steering projectors.

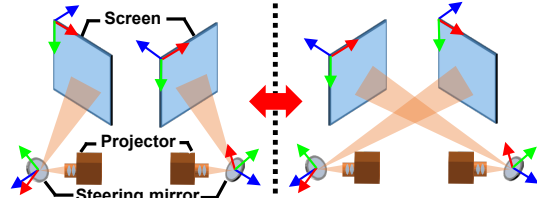


Fig. 6: Controlling dual steering projection. Assign the projectors and the screens facing angles close to each other in the front.

### 3.4.1 Mirror angle control

The algorithm for determining the steering mirror angle is described. Fig. 5 shows the projection control of a single steering projector. The angle of the steering mirror is determined so that the FoV center of the projector is aligned with the center of the screen.

Let  $\tilde{x}_C$  be the coordinate of the center of the screen in the camera coordinate system, and let  $\tilde{x}_P$  be the coordinate of the center pixel on the projector image plane. We estimate the specified angle  $\alpha, \beta$  of the mirror such that  $\tilde{x}_C$  is re-projected to  $\tilde{x}_P$ . The projective geometry from  $\tilde{x}_C$  to  $\tilde{x}_P$  can be expressed as:

$$\tilde{x}'_P \sim K_P D_P \left( [R_{MP}|t_{MP}] M(n, l) \begin{bmatrix} R_{CM} & t_{CM} \\ 0 & 1 \end{bmatrix} \tilde{x}_C \right). \quad (10)$$

First, derive the initial values of  $\alpha, \beta$ . For the initial value calculation, the distortion coefficient  $D_P(\cdot)$  and mirror thickness  $l$  are approximated to 0, and the following equation is obtained by deforming Eq. (10).

$$R_{MP}^T K_P^{-1} \tilde{x}_P - R_{MP}^T t_{MP} \sim M_r(n) [R_{CM}|t_{CM}] \tilde{x}_C. \quad (11)$$

Let the unit vector  $n_{ref}, n_{inc}$  be the left side and part of the right side of Eq. (11), as:

$$n_{inc} \sim R_{MP}^T K_P^{-1} \tilde{x}_P - R_{MP}^T t_{MP}, \quad n_{ref} \sim [R_{CM}|t_{CM}] \tilde{x}_C. \quad (12)$$

For the mirror surface's normal vector  $n$ , the relation between the incident vector  $n_{inc}$  and the reflection vector  $n_{ref}$  is established. From the geometric relationship between the incident vector, reflection vector and normal vector,  $n$  can be expressed as:

$$n = (n_{ref} - n_{inc}) / (\|n_{ref} - n_{inc}\|). \quad (13)$$

Let  $n = [n_x, n_y, n_z]^T$ , the initial values of  $\alpha, \beta$  are obtained from Eq. (6). By solving the following nonlinear optimization problem using the initial values,  $\alpha, \beta$  can be obtained.

$$\arg \min_{\alpha, \beta} d(\tilde{x}_P, \tilde{x}'_P)^2. \quad (14)$$

### 3.4.2 Conversion of target image

As shown in Fig. 5, the target image is transformed so that the corners of the target image and the corners of the screen coincide. Let  $\tilde{x}_{C\{q\}}$  be the coordinates of the corners of the projection area in the camera coordinate system and  $\tilde{x}_{C\{q\}}$  be the coordinates of the corners on the projector image plane, where  $q$  denotes the position of the corners.  $\tilde{x}_{C\{q\}}$  is obtained by reprojecting  $\tilde{x}_{C\{q\}}$  onto the projector image plane by Eq. (10). The target image is homographically transformed to fit a rectangle with the four corners  $\tilde{x}_{C\{q\}}$ .

### 3.4.3 Projection with multiple steering projectors

In this paper, it is assumed that one steering projector is used for one projection screen. In this case, when there are multiple candidates for steering projectors that can project to one screen, it is necessary to have an assignment criterion for which steering projector to use. In this paper, as shown in Fig. 6, we adopted the criterion of assigning the steering projector closest to the front-facing angle between the steering projector and the screen. Other allocation criteria, projection from multiple steering projectors on a single screen are discussed in Sec. 6.4.

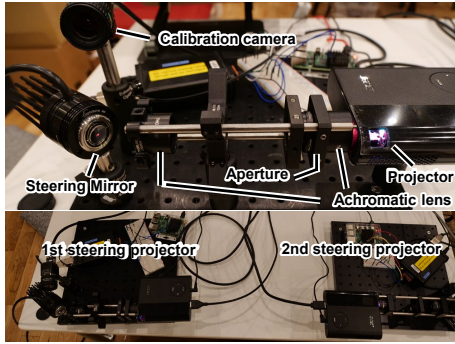


Fig. 7: Top: Single steering projector setup. The optical center of the projector is shifted over the mirror surface of the steering mirror by two achromatic lenses. The steering projector is also calibrated using a non-coaxial calibration camera. Bottom: Setup of two steering projectors.

Let  $n_{C\{m\}}$  be the inverse of the screen's normal vector in the camera coordinate system where  $m$  denotes the index of the screen. The normal  $n_{P\{m\}}$  in the projector coordinate system when the steering mirror angle  $(\alpha, \beta) = (0, 0)$  can be obtained from Eq. (8), as:

$$n_{P\{m\}} = [R_{MP\{n\}} | t_{MP\{n\}}] M(e_{-z}, l_{\{n\}}) \begin{bmatrix} R_{CM\{n\}} & t_{CM\{n\}} \\ 0 & 1 \end{bmatrix} n_{C\{m\}}, \quad (15)$$

where  $n$  is the index of the steering projector. Since  $e_z = [0, 0, 1]^T$  for the projector's line of sight, the angle  $\theta_{\{mn\}}$  that the steering projector and projection screen face is the angle formed by  $e_z$  and  $n_{P\{m\}}$ . The closer  $\theta_{\{mn\}}$  is to  $0^\circ$ , the closer the angle between the steering projector and the projection screen to the front. If there is one screen  $m$ , assign a steering projector  $n$  that satisfies:

$$\arg \min_n \theta_{\{mn\}}. \quad (16)$$

Consider the case where there is more than one screen  $m$ . Let  $\Omega(\cdot)$  be the current assignment of the screens and steering projectors and  $\Omega'(\cdot)$  be the other candidate assignment, where  $\Omega(\cdot), \omega'(\cdot)$  are function that returns the index of the steering projector from the index of the screen. When the following is satisfied for all screens  $m$  in the set of screen indices  $\mathbb{M}$ , the assignment is changed to  $\Omega'(\cdot)$ ,

$$\forall m \in \mathbb{M} : \theta_{\{m\Omega(m)\}} > \theta_{\{m\Omega'(m)\}}. \quad (17)$$

## 4 IMPLEMENTATION

To demonstrate our cooperative steering optics design and the calibration model, we implemented two prototypes based on two common tracking paradigms, inside-out and outside-in tracking.

The first one, the inside-out version, involves using the camera used for Projector-Camera System calibration directly for projection surface tracking. This system comprises steering projectors, cameras, and screens for projection targets. This prototype is to show the potential of spatial accuracy of our design.

The second one, the outside-in version, aimed at demonstrating the low latency potential of our design. This system is configured by adding a motion capture system to the first system. The steering projectors are described in Sec. 4.1, the two different methods of tracking are described in Sec. 4.2, and the screens are described in Sec. 4.3.

### 4.1 Steering projector

As shown in Fig. 7, two steering projectors consisting of a projector, a steering mirror, and two corresponding calibration cameras are installed. They are referred to as the 1st and 2nd steering projector, respectively. The hardware and software configuration is identical for the two steering projectors unless otherwise specified.

#### 4.1.1 Setup

For the steering projector, we used an Acer C200 projector (resolution:  $854 \times 480$  pixels) and an Optotune MR-E-2 steering mirror (mirror diameter: 15 mm, circular FoV: 25 rad, sensor resolution:  $22 \mu\text{rad}$ ). We removed the objective lens built into the projector, then placed two achromatic lenses (Thorlabs AC254-030-A-ML  $\times 2$ ) on the optical axis to shift the optical center of the projector on the mirror surface of the steering mirror. An aperture (Thorlabs SM1D12D) is placed between the two achromatic lenses to avoid internal reflections caused by wide-angle projector light.

The Raspberry Pi 4 Model B computer controls the steering mirror through SPI communication with the steering mirror driver board. The UDP and SPI communication programs were written in Rust. For the steering projector, we used a Windows 11 computer (Intel Core i9-8950HK CPU 2.90 GHz, 16.0 GB RAM, NVIDIA GeForce GTX 1080).

#### 4.1.2 Calibration

We placed the calibration camera, Ximea MQ042RG-CM, non-coaxially on the steering projector. A Computar M0814-VSW C-mount lens is used for the 1st steering projector and a Kowa LM12HC for the 2nd steering projector.

We computed the parameters in Tab. 1 at each steering projector based on the method described in Sec. 3.3,

First, we shot and projected calibration patterns following Sec. 3.3.1. We used a chessboard pattern (number of grids:  $13 \times 9$ , grid size: 1.9 mm) for calibration. For projection, we used a phase-shifting method [14] that employs a sinusoidal pattern as the structured light pattern. Since we need initial angles that can roughly project the pattern in the specified area, we manually set the initial mirror angles and scanned the surrounding specified angle.

Next, we applied bundle adjustment to the capture data. The normal camera calibration described in Sec. 3.3.2 was performed based on data shot separately using the same chessboard. Also, 50 mirror angles and pattern poses combinations were selected for the projector calibration. Then, initial value calculation (Sec. 3.3.4) and bundle adjustment (Sec. 3.3.3) were performed using the data taken at  $10 \sim 20$  different mirror angles for 20 different pattern poses, respectively. The projector's distortion coefficient  $D_P(\cdot)$  was assumed to be 0.

We implemented programs for camera capture and calibration in Python. We used OpenCV [3] for camera calibration and SciPy for optimization for which we set the default values defined in the `leastsq()` function. It should be noted here that our calibration method is versatile and can be used when some hardware is replaced.

#### 4.1.3 Projection control

Our system control each steering projector based on the method described in Sec. 3.4. The PC for steering projectors performs projection control in three threads. The first thread receives position and rotation data from the tracking program. The second thread calculates the angle of each steering mirror and sends the specified angle via UDP. Finally, the third thread calculates 2D homography on each projector. The projection control program was written in Python. Receiving data from the tracking program is described in Sec. 4.2.

## 4.2 Tracking Methods

As we mentioned, we implemented two prototypes with two standard tracking paradigms: inside-out and outside-in tracking. The first method involves using the camera employed for calibration to perform pose estimation of ArUco markers [20]. The second method utilizes a motion capture system for tracking the projection surface.

#### 4.2.1 Inside-out tracking-based Setup

In our first implementation, we utilized the pose estimation of ArUco markers. The camera used for ArUco markers detection was the Ximea MQ042RG-CM, which was also employed in the Projector-Camera System calibration. Fig. 9(b) shows the board with printed  $2 \times 2$  ArUco markers on the projection surface. The obtained pose of the projection surface was sent to the steering projector PC.

#### 4.2.2 Outside-in tracking-based Setup

In the current inside-out tracking prototype, we had to reduce ambient light to enhance the clarity of the projector's images. However, doing so requires increasing the exposure time of the camera used for ArUco markers detection, which can result in an increase in latency as a consequence. To address this latency issue, we also implemented a solution by introducing an outside-in motion capture system.

As an outside-in motion capture system to track the screen, we set up an OptiTrack system consisting of five OptiTrack PrimeX 22 tracking cameras. These tracking cameras have a built-in strobe light that emits infrared light, which enables high-speed tracking by capturing the reflected light from the retroreflective markers. Fig. 9(a) shows the setup of the tracking camera.

The tracking cameras send the captured frames via Ethernet to a server (Intel Core i5-10600 CPU 3.30 GHz, 16.0 GB RAM). The server processes the frames to detect retroreflective markers and performs 6DoF pose estimation via OptiTrack Motive software. The server streams the pose to the local network via UDP communication and the steering projector PC receives it via NatNet SDK.

We took one of the five tracking cameras for stereo calibration with the steering projector's calibration camera. This allows the motion capture system to control the projection of the camera coordinate system onto the screen, as described in Sec. 3.4. We used a circle grid (number of grids:  $11 \times 4$ , grid size: 60 mm) for stereo calibration with Python and OpenCV.

#### 4.3 Passive screen

Fig. 9(b) and (c) show the setup and optics of the passive screen. The passive screen uses a board and headset. The board consists of an A4 size projection area, and four ArUco markers.

The passive headset consists of birdbath optics, a diffusive screen, and a mirror. Birdbath optics are commonly used in AR-NEDs [12]. The birdbath optics were obtained by disassembling the AR headset Lenovo Mirage Solo. The obtained birdbath optics were reinforced with 3D printed parts, and a diffusive screen and mirror were attached to create a passive headset.

From a steering projector placed on a desk, which is lower than the height of the headset, the projection light is projected onto the diffusive screen of the passive headset by reflecting the projection light onto the mirror. The projected light reaching the diffusion screen enters the user's view through a beam splitter and beam combiner in the birdbath optic. The user can see an area of  $30 \text{ mm} \times 20 \text{ mm}$  (active area) on the diffusive screen for each eye.

Retroreflective markers are placed on the passive board and passive headset and tracked by OptiTrack. The offset between the retroreflective markers and the passive screen is calibrated by taking a picture of the ArUco marker on the screen from a calibration camera of the steering mirror and estimating its position and pose. During offline calibration of the passive headset, the ArUco markers were affixed on the diffusive screen and shot through the mirror.

Regarding the quality of the projected image, it is considered equivalent in terms of hardware setup to the existing beaming display, so evaluations such as Modulation Transfer Function (MTF) are also presumed to be comparable [7].

### 5 EVALUATION

We evaluate our system's projection accuracy and latency then showcases several potential benefits of our system beyond extending the presentation volume. We used the ArUco markers detection-based implementation for evaluating projection accuracy, and for subsequent evaluations, we utilized the motion capture system.

#### 5.1 Projection accuracy

We first evaluated our system's projection accuracy, including calibration and projection control algorithms between the steering projector, the camera, and a passive screen.

A sinusoidal pattern is projected towards a passive board and captured by an evaluation camera which was used for calibration between

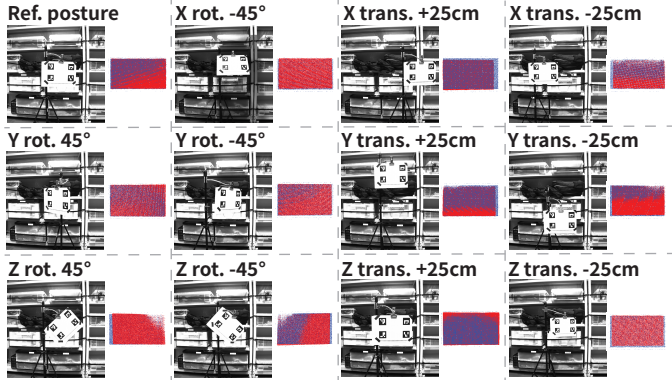


Fig. 8: Results of projection accuracy evaluation. For each pair, the left shows a picture taken from the evaluation camera for each passive board position and pose. The right shows the reprojected image of the projector pixel's true value (blue) and observed value (red). The mean error of all pixels of the projector is shown.

itself and the steering projector. This camera was also used for detection of ArUco markers. From the sinusoidal patterns and the ArUco markers, we obtain the observed values of where each projector pixel was projected on the screen and compare them with the true values to evaluate the projection error. Fig. 8 shows the images taken from the evaluation camera when the passive board was placed in 12 different positions and poses. The figure shows the observed and true values reprojected onto the screen and the mean error for all pixels. The reference posture of the passive board was the front face 1 m away from the steering projector and was translated  $\pm 25 \text{ cm}$  and rotated  $\pm 45^\circ$  about the xyz axes shown in Fig. 9.

The mean errors of all observed pixels were  $1.8 \sim 5.7 \text{ mm}$  with the average error of  $3.3 \text{ mm}$ . Considering that the active area of the passive headset is  $20 \text{ mm} \times 30 \text{ mm}$ , this accuracy is sufficient for image presentation within the user's field of view. However, as an ultimate goal, sub-millimeter accuracy may be needed depending on use cases. Factors affecting to decreasing accuracy and ways to improve it are discussed in Sec. 6.1.

Fig. 10(a) shows the viewpoint images projected to the passive headset in seven different positions and poses using the prototype with motion capture system. We observe that the target image is projected within the active area of the headset.

#### 5.2 Projection latency

Next, we evaluated the delay of the projection control algorithm (Fig. 11). The delay of the motion capture system (camera frame transmission, pose estimation, pose data transmission) is 7.2157 ms, the delay of mirror angle update is 7.2473 ms, the delay of target image update is 8.0493 ms are included in this system's delay. Full latency data of the experiment is in Table 2 in Appendix F.

When the projected image is incident on the active area of the passive headset, the maximum allowable movement velocity of the headset is about  $1.3828 \text{ m/s}$ . Also, assuming a head-turning radius of 40 cm, the maximum allowable angular velocity is about  $198.08 \text{ }^\circ/\text{s}$ . Improvements in projection latency are discussed in Sec. 6.2.

#### 5.3 Application of multiple steering projectors

In this section, we first show that two steering projectors can indeed extend the head orientation. Secondly, we also show and discuss that multiple steering projectors can realize more advanced applications beyond the extension such as for multiple users, improving dynamic range, binocular projection, etc.

##### 5.3.1 Head orientation extension

We show that two steering projectors can extend the head orientation of the passive headset. Based on the method described in Sec. 3.4.3, the steering projector facing more directly toward the passive screen

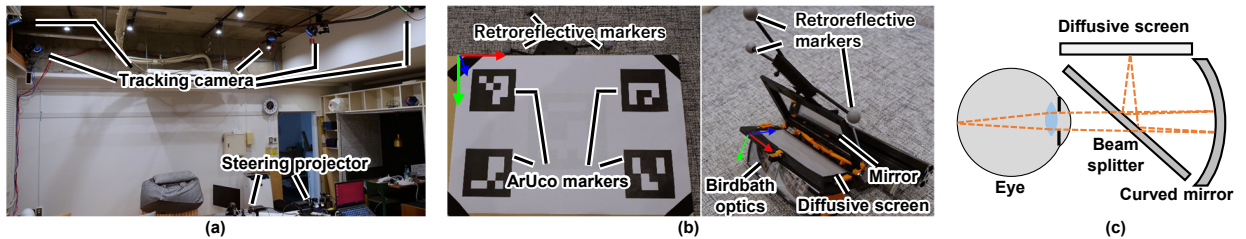


Fig. 9: (a) Setup of the outside-in tracking cameras and the dual steering projectors. (b) Setup of the passive board. Retroreflective markers are used for tracking, and ArUco markers [20] are used for calibration and evaluation. Middle: Setup of the passive headset. The projected light from the steering projector is reflected by the mirror and then projected onto the diffusive screen, which enters the user's eyes through birdbath optics. (c) Birdbath optics. Light projected onto the diffusive screen enters the user's eye through a beam splitter and beam combiner.

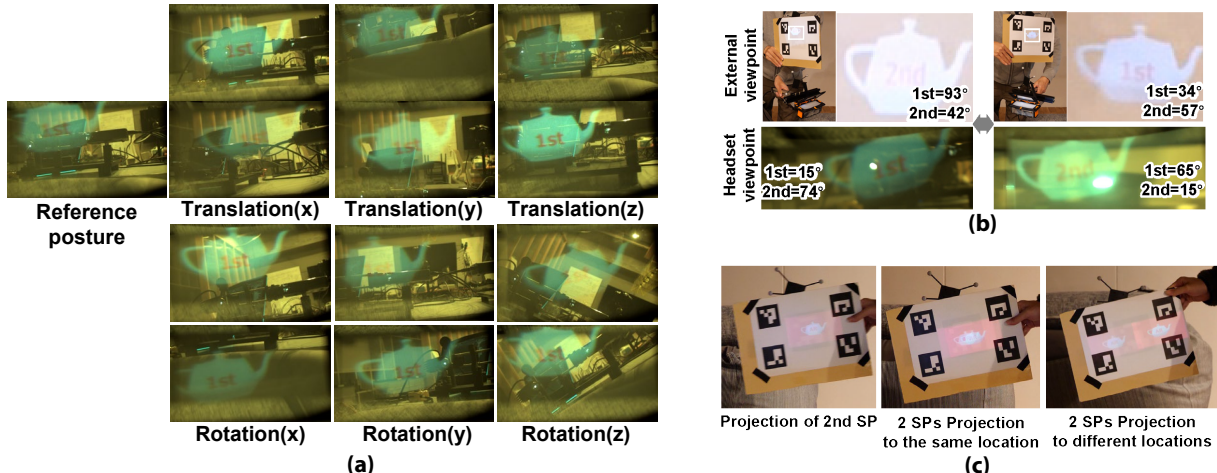


Fig. 10: Display results. (a) Viewpoint images when the headset's pose is changed. (b) Projection using two steering projectors (SPs) and two screens. The steering projectors (SPs) and screens are assigned to each other with their angles close to the front. The angle between the SPs and the screens are presented. (c) Left: Projection from the 2nd steering projector (SP) onto the passive board. Middle: Two SPs projecting to the same location (improved dynamic range). Right: Two SPs projecting to different locations (binocular presentation).

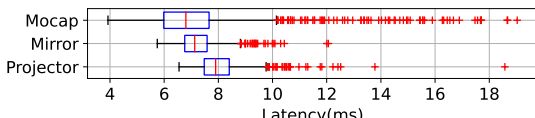


Fig. 11: Boxplot of the latency measurement of the motion capture system, the steering mirror, and the projector.

is selected for projection. The steering projector that is not selected should not project to the screen by turning the steering mirror angle downward.

Fig. 10(b) shows the projection when the passive headset is rotated. In passive headset orientation A, the angle with the 1st SP is  $18^\circ$  and with the 2nd SP is  $55^\circ$ . In orientation B, the angle with the 1st SP is  $62^\circ$  and the angle with the 2nd SP is  $8^\circ$ . The steering projector is switched based on the orientation of the passive headset, indicating that the head orientation is extended.

### 5.3.2 Multiple users

Two steering projectors are used to project two passive screens to demonstrate the potential for multiple-user applications. Based on the method described in Sec. 3.4.3, a near frontal allocation is maintained by timely swapping the allocation between the steering projectors and the passive screens depending on the angle.

Fig. 10(b) shows the projection onto the passive board and the passive headset using two steering projectors. Initially, the passive board and the passive headset are assigned to separate steering projectors. Then, when each passive screen is turned toward the steering projector of the one that is not assigned, the allocation of steering projectors is swapped. This shows that the images are presented while assigning the

steering projector closer to the front to the multiple screens.

### 5.3.3 Dynamic range improvement

We demonstrate the potential for improved dynamic range by applying multiple steering projectors. The dynamic range can be improved by projecting to the same location for one passive screen, as shown in Fig. 10(c)(middle). However, higher calibration accuracy is needed because the two projection positions should coincide to properly improve the dynamic range.

### 5.3.4 Binocular presentation

We demonstrate the potential for binocular presentation by applying multiple steering projectors. As shown in Fig. 10(c)(right), the binocular presentation can be realized by projecting to two ranges for a single passive screen. For proper depth presentation by binocular disparity, it is necessary to control the projection according to the user's eye position.

## 6 DISCUSSION AND FUTURE WORK

There is room to improve this system toward a more practical distributed beaming display system. In this section, we discuss the challenges of the current system and directions for future work.

### 6.1 Projection accuracy

As noted in Sec. 5.1, the current system has a projection error of  $1.8 \sim 5.7$  mm at a distance of about 1 m from the steering projector. This projection error is a combination of calibration and tracking errors. Particularly, steering projectors' calibration errors are considered significant. This is due to the difficulty in accurately detecting the

projector pixels from the calibration camera because of the projector's small angle of view and depth of field.

Two policies to improve calibration accuracy can be identified. The first is to detect the projector pixels accurately. Sueishi et al. used a calibration pattern with retroreflective sheets and coaxial illumination to achieve highly accurate detection of calibration points for a system consisting of a camera and a galvanometer mirror [27]. This system also has the potential to detect projector pixels with high accuracy by coaxially placing an additional calibration camera on the steering projector and projecting a structured light pattern against a calibration pattern using retroreflective sheets. Elsewhere, Sugimoto et al. proposed a focal-distance-independent projector calibration using a pinhole array [29]. This method may improve detection accuracy because it reduces out-of-focus while placing the calibration pattern close to the steering projector.

The second is to perform feedback control based on the image of the steering projector. Existing DPM [16, 17, 24, 28] and beaming displays [7] control the mirror angle by PID control from the 2D offset between the projection target and the image. In this system, too, highly accurate projection can be expected by using 2D offset for projection control of a single steering projector and 3D tracking for coordination of multiple steering projectors. To fine-tune the calibration parameters, observation-based approach such as camera-in-the-loop methods may be considered [4, 25].

## 6.2 Projection latency

The projection latency compromises comfort because when the user moves their head, the target image is presented late from the intended position [10]. System delays include tracking, computational, display, steering, and transmission delays.

Regarding tracking latency, the system uses infrared tracking with retroreflective markers, which is faster than the tracking with visible markers used in the existing beaming display [7]. To further improve the tracking latency, our system may be possible to apply fast-tracking using a duo-lateral linear photodiode [2]. Using this photodiode, Hiroi et al. implemented a low-latency beaming display with a motion-to-photon latency of 133  $\mu$ s [6].

Also, the computational latency can be improved by improving the efficiency of calculating the mirror specification angle and the objective image transformation algorithm and modularized parallel computing for each steering projector. Furthermore, for the display latency, a high frame rate projector [33] and an image display correction technique based on tracking data [13] can be applied. Finally, regarding transmission delays, this system extensively uses network communications to link multiple projectors, steering mirrors, and a motion capture system. Replacing these transmissions with analog signals is expected to reduce transmission latency.

## 6.3 Focus, light intensity and resolution

In the current system, as the distance between the steering projector and the screen changes, the focus, light intensity, and resolution of the projected image change. This is because the projector's projection optics are fixed focus, and the angle of view is constant. Two policies can be identified to ensure these projection qualities do not change. The first is to use a variable focus lens [31]. Wang et al. dynamically controlled the projector's focal length using a variable focus lens [32]. The existing beaming display [7] also dynamically focuses according to the distance between the steering projector and the passive headset. By using two variable focus lenses, it is possible to control not only dynamic focusing but also light intensity and resolution by dynamically changing the angle of view. However, accurate projection alignment requires a modeling and calibration method for the steering projector, including the variable focus lenses. The second method is to use a laser scanning projector [9]. Since laser light is used, the image is not out of focus, regardless of the distance from the projection screen. Suppose the scanning range of the laser light is controlled based on the tracking data of the projection screen. In that case, a constant light intensity and resolution presentation can be realized in principle regardless of the distance from the projection screen.

## 6.4 Multiple steering projectors

### 6.4.1 Steering projector and screen assignment criteria

As described in the Sec. 3.4.3, the steering projectors and screens assignment in this system is based on the angle they make. While this assignment criterion effectively projects correctly for head rotation, it does not consider the distance between the steering projector and the projection screen. For example, suppose multiple steering projectors are installed in the far and near directions; in that case, the light intensity and resolution may be higher if the near steering projector is assigned to the far steering projector, even if the angle with the far steering projector is smaller than that with the near one. Therefore, to have the steering projectors widely distributed over the space, it is necessary to have allocation criteria that include distance. In addition, when multiple users utilize this system, there is a possibility that one projector may be contested among users. Therefore, if a projector is already assigned to one user, it is necessary to establish criteria to assign other projectors to different users.

The size of the target image after image transformation (Sec. 3.4.2) is effective as an allocation criterion that considers the distance between the steering projector and the screen. The larger the size of the target image, the greater the projected image's light intensity and resolution since the projector's FoV is widely utilized. Therefore, high projection quality can be maintained by assigning a steering projector with a larger target image after image conversion.

In addition, assigning another steering projector when there is a blockage between the steering projector and the projection screen is also worth considering when putting the beaming display system into practical use.

### 6.4.2 Color compensation

This paper focuses on geometric alignment for the cooperative control of multiple steering projectors. In addition, color compensation should also be considered in the cooperative control. For example, when the steering projectors assigned to a screen are switched, the color characteristics of each projector are different, resulting in a change in the target image's color. Therefore, to make the user unaware of the switching of assignments, it is necessary to calibrate the color characteristics of each projector.

In addition, in this system, the screen and steering projector assignment is one-to-one. However, when multiple steering projectors are assigned to a single screen, a blending method is needed to reduce artifacts caused by overlapping projection areas. Nomoto et al. proposed a blending method for dynamic projection mapping that uses a parallel pixel computation and parallel computing [22]. Such a blending method can be applied to beaming display systems with multiple steering projectors.

### 6.4.3 Applications

In the Sec. 5.3, we listed the following applications of beaming display with multiple steering projectors: head orientation and projection volume expansion, multiple users, dynamic range improvement, and binocular presentation. Another application is resolution enhancement.

There are several prior studies on resolution enhancement by multiple projectors, which can be divided into three types. The first is the tiling of multiple projected images. The second is a super-resolution technique that uses the superimposition of projected images. The third is a method in which a wide/low-resolution projection is made in the peripheral FoV, and a narrow/high-resolution projection is made in the central FoV, considering that human visual acuity is higher near the fovea [8]. This requires dynamic projection control based on the direction of the user's eyes and is considered compatible with a beaming display, which uses a steering projector.

## 7 CONCLUSION

In this study, we proposed a dual-beaming display system that extends the head orientation and projection volume by dual steering projectors. We derived a formal model and the calibration procedure of dual steering projectors with steerable mirrors and an outside-in tracking

system. The model and the calibration procedure are also designed to be scalable to multiple beaming display setups.

The experiments revealed that a single steering projector provided about 1.8~5.7 mm and 14.46 ms accuracy and latency, respectively, at the projection distance of about 1 m from the passive headset. Additionally, we demonstrated that multiple steering projectors could extend the head orientation, support multiple users, increase dynamic range, and enable binocular presentation as possible applications. We further discussed, for future work, guidelines for improving the performance of steering projectors and how to coordinate multiple steering projectors.

## SUPPLEMENTAL MATERIALS

All supplemental materials including data and code will be available on Open Science Framework at [*the link is omitted for the blind review*] released under a CC BY 4.0 license. In particular, they include (1) source code, (2) experimental results, (3) materials for the figures used in this paper, and (4) a full version of this paper with all appendices.

## ACKNOWLEDGMENTS

This work was supported in part by JST FOREST Grant Number JP-MJFR206E, and JSPS KAKENHI Grant Number JP21K19788 and JP20H05958, Japan.

## REFERENCES

- [1] K. Akşit and Y. Itoh. Holobeam: Paper-thin near-eye displays. *arXiv preprint arXiv:2212.05057*, 2022. 1
- [2] A. Blate, M. Whitton, M. Singh, G. Welch, A. State, T. Whitted, and H. Fuchs. Implementation and evaluation of a 50 khz, 28 $\mu$ s motion-to-pose latency head tracking instrument. *IEEE TVCG*, 25(5):1970–1980, 2019. doi: 10.1109/TVCG.2019.2899233 8
- [3] G. Bradski. The opencv library. *Dr. Dobb's Journal: Software Tools for the Professional Programmer*, 25(11):120–123, 2000. 5
- [4] P. Chakravarthula, E. Tseng, T. Srivastava, H. Fuchs, and F. Heide. Learned hardware-in-the-loop phase retrieval for holographic near-eye displays. *ACM Transactions on Graphics (TOG)*, 39(6):1–18, 2020. 8
- [5] D. A. Forsyth and J. Ponce. Computer vision, a modern approach. prentice hall. *Upper Saddle River*, 2003. 3
- [6] Y. Hiroi, A. Watanabe, Y. Mikawa, and Y. Itoh. Low-latency beaming display: Implementation of wearable, 133 $\mu$ s motion-to-photon latency near-eye display. *IEEE Transactions on Visualization and Computer Graphics*, 29(11):4761–4771, 2023. doi: 10.1109/TVCG.2023.3320212 8
- [7] Y. Itoh, T. Kaminokado, and K. Akşit. Beaming displays. *IEEE TVCG*, 27(5):2659–2668, 2021. doi: 10.1109/TVCG.2021.3067764 1, 2, 6, 8
- [8] D. Iwai, K. Kodama, and K. Sato. Reducing motion blur artifact of foveal projection for a dynamic focus-plus-context display. *IEEE Transactions on Circuits and Systems for Video Technology*, 25(4):547–556, 2015. doi: 10.1109/TCSVT.2014.2352500 8
- [9] Y. Kitajima, D. Iwai, and K. Sato. Simultaneous projection and positioning of laser projector pixels. *IEEE TVCG*, 23(11):2419–2429, 2017. doi: 10.1109/TVCG.2017.2734478 8
- [10] G. A. Koulieris, K. Akşit, M. Stengel, R. K. Mantiuk, K. Mania, and C. Richardt. Near-eye display and tracking technologies for virtual and augmented reality. In *Computer Graphics Forum*, vol. 38, pp. 493–519. Wiley Online Library, 2019. 1, 2, 8
- [11] B. Kress and T. Starner. A review of head-mounted displays (hmd) technologies and applications for consumer electronics. *Photonic Applications for Aerospace, Commercial, and Harsh Environments IV*, 8720:62–74, 2013. 2
- [12] B. C. Kress. Optical waveguide combiners for AR headsets: features and limitations. In B. C. Kress and P. Schelkens, eds., *Digital Optical Technologies 2019*, vol. 11062, p. 110620J. International Society for Optics and Photonics, SPIE, 2019. doi: 10.1117/12.2527680 6
- [13] P. Lincoln, A. Blate, M. Singh, T. Whitted, A. State, A. Lastra, and H. Fuchs. From motion to photons in 80 microseconds: Towards minimal latency for virtual and augmented reality. *IEEE TVCG*, 22(4):1367–1376, 2016. doi: 10.1109/TVCG.2016.2518038 8
- [14] M. Maruyama, S. Tabata, Y. Watanabe, and M. Ishikawa. Multi-pattern embedded phase shifting using a high-speed projector for fast and accurate dynamic 3d measurement. In *2018 IEEE Winter Conference on Applications of Computer Vision (WACV)*, pp. 921–929, 2018. doi: 10.1109/WACV.2018.00106 5
- [15] Y. Mikawa, M. Fujiwara, T. Hiraki, Y. Makino, and H. Shinoda. Far-field aerial image presentation of one point by a laser source using beam scanning by two-axis galvanometer mirror. In *2021 60th Annual Conference of the Society of Instrument and Control Engineers of Japan (SICE)*, pp. 137–143. IEEE, 2021. 2
- [16] Y. Mikawa, T. Sueishi, Y. Watanabe, and M. Ishikawa. Varielight: Hybrid dynamic projection mapping using high-speed projector and optical axis controller. In *SIGGRAPH Asia 2018 Emerging Technologies*, SA '18. Association for Computing Machinery, New York, NY, USA, 2018. doi: 10.1145/3275476.3275481 2, 8
- [17] Y. Mikawa, T. Sueishi, Y. Watanabe, and M. Ishikawa. Dynamic projection mapping for robust sphere posture tracking using uniform/biased circumferential markers. *IEEE TVCG*, 28(12):4016–4031, 2022. doi: 10.1109/TVCG.2021.3111085 2, 8
- [18] J. J. Moré. The levenberg-marquardt algorithm: implementation and theory. In *Numerical analysis*, pp. 105–116. Springer, 1978. 4
- [19] D. Moreno and G. Taubin. Simple, accurate, and robust projector-camera calibration. In *2012 Second International Conference on 3D Imaging, Modeling, Processing, Visualization & Transmission*, pp. 464–471, 2012. doi: 10.1109/3DIMPVT.2012.77 3, 4
- [20] R. Munoz-Salinas and S. Garrido-Jurado. Aruco library. URL: <http://sourceforge.net/projects/aruco>, 2013. 5, 7
- [21] M. Nitta, T. Sueishi, and M. Ishikawa. Tracking projection mosaicing by synchronized high-speed optical axis control. In *Proceedings of the 24th ACM Symposium on Virtual Reality Software and Technology*, VRST '18. Association for Computing Machinery, New York, NY, USA, 2018. doi: 10.1145/3281505.3281553 2
- [22] T. Nomoto, W. Li, H. Peng, and Y. Watanabe. Dynamic multi-projection mapping based on parallel intensity control. *IEEE Transactions on Visualization & Computer Graphics*, 28(05):2125–2134, may 2022. doi: 10.1109/TVCG.2022.3150488 2, 8
- [23] K. Okumura, H. Oku, and M. Ishikawa. High-speed gaze controller for millisecond-order pan/tilt camera. In *2011 IEEE International Conference on Robotics and Automation*, pp. 6186–6191, 2011. doi: 10.1109/ICRA.2011.5980080 2
- [24] K. Okumura, H. Oku, and M. Ishikawa. Active projection ar using high-speed optical axis control and appearance estimation algorithm. In *2013 IEEE International Conference on Multimedia and Expo (ICME)*, pp. 1–6, 2013. doi: 10.1109/ICME.2013.6607637 2, 8
- [25] Y. Peng, S. Choi, N. Padmanaban, and G. Wetzstein. Neural holography with camera-in-the-loop training. *ACM Transactions on Graphics (TOG)*, 39(6):1–14, 2020. 8
- [26] C. Siegl, M. Colaianni, L. Thies, J. Thies, M. Zollhöfer, S. Izadi, M. Stammer, and F. Bauer. Real-time pixel luminance optimization for dynamic multi-projection mapping. *ACM Trans. Graph.*, 34(6), nov 2015. doi: 10.1145/2816795.2818111 2
- [27] T. Sueishi, H. Oku, and M. Ishikawa. Mirror-based high-speed gaze controller calibration with optics and illumination control. In *2015 IEEE/RSJ International Conference on Intelligent Robots and Systems (IROS)*, pp. 3064–3070, 2015. doi: 10.1109/IROS.2015.7353800 2, 8
- [28] T. Sueishi, H. Oku, and M. Ishikawa. Robust high-speed tracking against illumination changes for dynamic projection mapping. In *2015 IEEE Virtual Reality (VR)*, pp. 97–104, 2015. doi: 10.1109/VR.2015.7223350 2, 8
- [29] M. Sugimoto, D. Iwai, K. Ishida, P. Punpongsan, and K. Sato. Directionally decomposing structured light for projector calibration. *IEEE TVCG*, 27(11):4161–4170, 2021. doi: 10.1109/TVCG.2021.3106511 8
- [30] D. Wan and J. Zhou. Stereo vision using two ptz cameras. *Computer Vision and Image Understanding*, 112(2):184–194, 2008. 2
- [31] L. Wang, H. Oku, and M. Ishikawa. An improved low-optical-power variable focus lens with a large aperture. *Opt. Express*, 22(16):19448–19456, Aug 2014. doi: 10.1364/OE.22.019448 8
- [32] L. Wang, H. Xu, S. Tabata, Y. Hu, Y. Watanabe, and M. Ishikawa. High-speed focal tracking projection based on liquid lens. In *ACM SIGGRAPH 2020 Emerging Technologies*, SIGGRAPH '20. Association for Computing Machinery, New York, NY, USA, 2020. doi: 10.1145/3388534.3408333 8
- [33] Y. Watanabe, G. Narita, S. Tatsuno, T. Yuasa, K. Sumino, and M. Ishikawa. High-speed 8-bit image projector at 1,000 fps with 3 ms delay. In *22nd International Display Workshops, IDW 2015*, pp. 1421–1422. International Display Workshops, 2015. 8
- [34] A. Wilson, H. Benko, S. Izadi, and O. Hilliges. Steerable augmented reality with the beamatron. In *Proceedings of the 25th annual ACM UIST*, pp. 413–422, 2012. 2
- [35] K. Yamamoto, D. Iwai, I. Tani, and K. Sato. A monocular projector-

- camera system using modular architecture. *IEEE TVCG*, pp. 1–9, 2022.  
doi: 10.1109/TVCG.2022.3217266 2
- [36] Z. Zhang. A flexible new technique for camera calibration. *IEEE Transactions on Pattern Analysis and Machine Intelligence*, 22(11):1330–1334, 2000. doi: 10.1109/34.888718 4

## SUPPLEMENTARY DOCUMENT FOR THE SUBMISSION:

### "Towards Co-operative Beaming Displays: Dual Steering Projectors for Extended Projection Volume and Head Orientation Range"

#### A TABLE OF VARIABLES

Table 1 summarizes calibration parameters used in Sec. 3.3.3.

#### B DERIVATION PROCESS OF INITIAL PARAMETERS IN SEC. 3.3.4

The following nonlinear optimization problem can calculate the initial value of  $R_{MP}$ .

$$\arg \min_{R_{MP}} \sum_{i_1, i_2, k} \|R_{OP\{i_1k\}} R_{OP\{i_2k\}}^T R_{MP} - R_{MP} M_r(n_{\{i_1\}}) M_r(n_{\{i_2\}})\|_F^2, \quad (18)$$

where  $\|\cdot\|_F^2$  is the Frobenius norm and  $i_1, i_2$  is the combination of two mirror angles in each pattern pose  $k$ . The detailed derivation process is summarized in Appendix C.

The following linear optimization problem can calculate the initial value of  $t_{MP}$ .

$$\arg \min_{t_{MP}} \|At_{MP} - b\|^2, \quad (19)$$

where  $A, b$  are the following  $A_{\{i_1i_2\}}, b_{\{i_1i_2\}}$  respectively, which are vertically combined for each  $i_1, i_2, k$ .

$$A_{\{i_1i_2\}} = \{M_r(n_{\{i_1\}}) - M_r(n_{\{i_2\}})\} R_{MP}^T, \quad (20)$$

$$b_{\{i_1i_2\}} = M_r(n_{\{i_1\}}) R_{MP}^T t_{OP\{i_1k\}} - M_r(n_{\{i_2\}}) R_{MP}^T t_{OP\{i_2k\}} + M_t(n_{\{i_1\}}, l) - M_t(n_{\{i_2\}}, l), \quad (21)$$

where  $R_{MP}$  is used the initial values obtained by Eq. (18). The detailed derivation process is summarized in Appendix D.

The initial value of  $R_{OM\{k\}}, t_{OM\{k\}}$  is averaged over the following equation for the projector posture  $i$ .

$$R_{OM\{k\}} = M_r(n_{\{i\}}) R_{MP}^T R_{OP\{ik\}} I_z, \quad (22)$$

$$t_{OM\{k\}} = M_t(n_{\{i\}}, l) + M_r(n_{\{i\}}) R_{MP}^T (t_{OP\{ik\}} - t_{MP}), \quad (23)$$

where  $R_{MP}, t_{MP}$  are used the initial values obtained by Eqs. (18) and (19). The detailed derivation process is summarized in Appendix E.

The initial value of  $R_{CM}, t_{CM}$  is averaged over the following equation for the pattern pose  $k$ .

$$R_{CM} = R_{OM\{k\}} R_{OC\{k\}}^T, \quad (24)$$

$$t_{CM} = t_{OM\{k\}} - R_{OM\{k\}} R_{OC\{k\}}^T t_{OC\{k\}}, \quad (25)$$

where  $R_{OM\{k\}}, t_{OM\{k\}}$  are used the initial values obtained by Eqs. (22) and (23). The detailed derivation process is summarized in Appendix E.

#### C DERIVATION PROCESS OF EQ. (18)

Comparing with the projective geometry of Sec. 3.2.1 in the projector and mirror model described in Sec. 3.3, the following equation holds.

$$[R_{MP}|t_{MP}] M(n_{\{i\}}, l) \begin{bmatrix} R_{OM\{k\}} & t_{OM\{k\}} \\ 0 & 1 \end{bmatrix} = [R_{OP\{ik\}} | t_{OP\{ik\}}] \begin{bmatrix} I_z & 0 \\ 0 & 1 \end{bmatrix} \quad (26)$$

Expanding the equation, we obtain the following equation.

$$[R_{MP} M_r(n_{\{i\}}) R_{OM\{k\}} | t_{MP} + R_{MP} M_t(n_{\{i\}}, l) + R_{MP} M_r(n_{\{i\}}) t_{OM\{k\}}] = [R_{OP\{ik\}} | t_{OP\{ik\}}] \quad (27)$$

Focusing on the rotational component of Eq. (27), we obtain the following equations for the mirror angles  $i_1, i_2$ .

$$R_{MP} M_r(n_{\{i_1\}}) R_{OM\{k\}} = R_{OP\{i_1k\}} I_z \quad (28)$$

$$R_{MP} M_r(n_{\{i_2\}}) R_{OM\{k\}} = R_{OP\{i_2k\}} I_z \quad (29)$$

Table 1: Calibration parameters

	Camera matrix	$K_C$
	Camera lens distortion	$D_C$
	Projector matrix	$K_P$
	Projector lens distortion	$D_P$
Estimated value	Camera to Mirror rotation	$R_{CM}$
	Camera to Mirror translation	$t_{CM}$
	Mirror to Projector rotation	$R_{MP}$
	Mirror to Projector translation	$t_{MP}$
Fixed value	Mirror thickness	$l$
	Calibration point(3D, Pattern)	$\tilde{x}_{O\{jk\}}$
Specified value	Mirror specified angle	$\alpha_{\{i\}}, \beta_{\{i\}}$
Observed value	Calibration point(2D, Camera)	$\tilde{x}_{C\{jk\}}$
	Calibration point(2D, Projector)	$\tilde{x}_{P\{ijk\}}$

By transforming the equations, we obtain the following equations.

$$R_{OP\{i_1k\}}^T R_{MP} M_r(n_{\{i_1\}}) = I_z R_{OM\{k\}}^T \quad (30)$$

$$R_{OP\{i_2k\}}^T R_{MP} M_r(n_{\{i_2\}}) = I_z R_{OM\{k\}}^T \quad (31)$$

Since the right-hand sides of the two equations coincide, we obtain the following equation.

$$R_{OP\{i_1k\}}^T R_{OP\{i_2k\}} R_{MP} - R_{MP} M_r(n_{\{i_1\}}) M_r(n_{\{i_2\}}) = 0 \quad (32)$$

By transforming the equation, we obtain the following equations

$$R_{OP\{i_1k\}} R_{OP\{i_2k\}}^T R_{MP} - R_{MP} M_r(n_{\{i_1\}}) M_r(n_{\{i_2\}}) = 0 \quad (33)$$

Therefore, the initial value of  $R_{MP}$  can be computed by the nonlinear optimization problem in Eq. (18).

#### D DERIVATION PROCESS OF EQ. (19)

Focusing on the translational component of Eq. (27), we obtain the following equations for the mirror angles  $i_1, i_2$ .

$$t_{MP} + R_{MP} M_t(n_{\{i_1\}}, l) + R_{MP} M_r(n_{\{i_1\}}) t_{OM\{k\}} = t_{OP\{i_1k\}} \quad (34)$$

$$t_{MP} + R_{MP} M_t(n_{\{i_2\}}, l) + R_{MP} M_r(n_{\{i_2\}}) t_{OM\{k\}} = t_{OP\{i_2k\}} \quad (35)$$

By transforming the equations, we obtain the following equations.

$$M_r(n_{\{i_1\}}) R_{MP}^T t_{OP\{i_1k\}} - M_r(n_{\{i_1\}}) R_{MP}^T t_{MP} + M_t(n_{\{i_1\}}, l) = t_{OM\{k\}} \quad (36)$$

$$M_r(n_{\{i_2\}}) R_{MP}^T t_{OP\{i_2k\}} - M_r(n_{\{i_2\}}) R_{MP}^T t_{MP} + M_t(n_{\{i_2\}}, l) = t_{OM\{k\}} \quad (37)$$

Since the right-hand sides of the two equations coincide, we obtain the following equation.

$$M_r(n_{\{i_1\}}) R_{MP}^T t_{OP\{i_1k\}} - M_r(n_{\{i_1\}}) R_{MP}^T t_{MP} + M_t(n_{\{i_1\}}, l) = \quad (38)$$

$$M_r(n_{\{i_2\}}) R_{MP}^T t_{OP\{i_2k\}} - M_r(n_{\{i_2\}}) R_{MP}^T t_{MP} + M_t(n_{\{i_2\}}, l)$$

By transforming the equation, we obtain the following equations

$$\{M_r(n_{\{i_1\}}) - M_r(n_{\{i_2\}})\} R_{MP}^T t_{MP} - \{M_r(n_{\{i_1\}}) R_{MP}^T t_{OP\{i_1k\}} - M_r(n_{\{i_2\}}) R_{MP}^T t_{OP\{i_2k\}} + M_t(n_{\{i_1\}}, l) - M_t(n_{\{i_2\}}, l)\} = 0 \quad (39)$$

$$-M_r(n_{\{i_2\}}) R_{MP}^T t_{OP\{i_2k\}} + M_t(n_{\{i_1\}}, l) - M_t(n_{\{i_2\}}, l) = 0$$

Therefore, the initial value of  $t_{MP}$  can be computed by the linear optimization problem in Eq. (19).

Table 2: Projection latency. (\*)Settling times indicated in the catalog specifications (e.g., 2 ms for  $0.1^\circ$ . and 12 ms for  $20^\circ$ .).

		Ave.	Std.
Mocap	Frame transmission	3.0865 ms	0.0793
	Pose estimation	0.5205 ms	0.2044
	Pose transmission	3.6087 ms	2.2413
	Total	7.2157 ms	2.2471
Mirror	Angle calculation	2.2908 ms	0.5034
	Angle transmission	2.9565 ms	0.5103
	Steering	2 ms *	n.a.
	Total	7.2473 ms	0.7182
Projector	Image transformation	5.2040 ms	0.6258
	Display	2.8453 ms	0.4183
	Total	8.0493 ms	0.8737

## E DERIVATION PROCESS OF Eqs. (22) TO (25)

By deformation the rotational and translational components of Eq. (27), Eqs. (22) and (23) can be obtained.

The conversion from O to M is equal to conversion from O to M via C. Therefore, we obtain the equation:

$$[R_{OM\{k\}}|t_{OM\{k\}}] = [R_{CM}|t_{CM}] \begin{bmatrix} R_{OC\{k\}} & t_{OC\{k\}} \\ 0 & 1 \end{bmatrix} \quad (40)$$

Expanding the equation, we obtain the following equation.

$$[R_{OM\{k\}}|t_{OM\{k\}}] = [R_{CM}R_{OC\{k\}}|t_{CM} + R_{CM}t_{OC\{k\}}] \quad (41)$$

By deformation the rotational and translational components of Eq. (41), Eqs. (24) and (25) can be obtained.

## F TABLE OF LATENCY VALUES

Table 2 that shows the mean and standard deviation of 1000 measurements of each delay of this system in Sec. 5.2.